

# Mixing and sorting of bidisperse two-dimensional bubbles

P.I.C. Teixeira<sup>1,2,a</sup>, F. Graner<sup>3</sup>, and M.A. Fortes<sup>2</sup>

<sup>1</sup> Faculdade de Engenharia, Universidade Católica Portuguesa, Estrada de Talaíde, P-2635-631 Rio de Mouro, Portugal

<sup>2</sup> Departamento de Engenharia de Materiais, e Instituto de Ciência e Engenharia de Materiais e Superfícies, Instituto Superior Técnico, Avenida Rovisco Pais, P-1049-001 Lisbon, Portugal

<sup>3</sup> CNRS UMR 5588 et Université Grenoble, Laboratoire de Spectrométrie Physique, Boîte Postale 87, F-38402 St. Martin d'Hères Cedex, France

Received 1 August 2002 /

Published online: 3 December 2002 – © EDP Sciences / Società Italiana di Fisica / Springer-Verlag 2002

**Abstract.** We have examined a number of candidates for the minimum-surface-energy arrangement of two-dimensional clusters composed of  $N$  bubbles of area 1 and  $N$  bubbles of area  $\lambda$  ( $\lambda \leq 1$ ). These include hexagonal bubbles sorted into two monodisperse honeycomb tilings, and various mixed periodic tilings with at most four bubbles per unit cell. We identify, as a function of  $\lambda$ , the minimal configuration for  $N \rightarrow \infty$ . For finite  $N$ , the energy of the external (*i.e.*, cluster-gas) boundary and that of the interface between honeycombs in “phase-separated” clusters have to be taken into account. We estimate these contributions and find the lowest total energy configuration for each pair  $(N, \lambda)$ . As  $\lambda$  is varied, this alternates between a circular cluster of one of the mixed tilings, and “partial wetting” of the monodisperse honeycomb of bubble area 1 by the monodisperse honeycomb of bubble area  $\lambda$ .

**PACS.** 83.80.Iz Emulsions and foams – 82.70.Rr Aerosols and foams – 02.70.Rr General statistical methods

## 1 Introduction

In spite of their ephemeral nature, foams have been inspiring scientists for some time. As is well known, a liquid foam is an assembly of gas bubbles bounded by liquid films. Besides occurring in some popular beverages, foams find many important industrial applications, ranging from food, toiletries and cleaning products, to fire fighting, oil recovery and mixture segregation by fractionation or flotation. In addition, metal foams are fast becoming useful engineering materials [1]. On a more fundamental note, aqueous foams, whose structure is surface-tension dominated, are a model for a class of systems in which the interfacial area (in three dimensions (3d)) or the perimeter (in two dimensions (2d)) is minimised at equilibrium. In particular, one might ask: how can space be partitioned into regions of equal volume (in 3d) or area (in 2d) such that there is the least amount of boundary? This puzzle of discrete geometry is known as the *Kelvin problem*. In 2d the solution is a honeycomb —as suspected since at least classical antiquity [2], but only very recently proved [3]. Things are trickier in 3d: Kelvin, in 1887 [4], proposed as lowest-energy structure a regular packing of what he called tetrakaidcahedra —truncated octahedra with slightly curved hexagonal faces. Kelvin’s conjecture stood for more than a century until it was bettered in 1994

by Weaire and Phelan [5], whose ordered arrangement of *two* types of polyhedron (of the same volume) has 0.2% lower energy. Still, as no rigorous proof exists that the latter is the division of space into equal cells with minimum partitioned area, the search goes on.

In the real world, however, foams consist of a finite number of bubbles with a distribution of sizes (*i.e.*, they are finite *and* polydisperse). Now that the Kelvin problem has been solved in 2d, it is natural to look at these two extensions thereof. In order to gain insight, we focus here on the most easily tractable case, and ask ourselves the question: what is the absolute minimum-energy configuration of a 2d bidisperse foam of a given composition (expressed in terms of the numbers and sizes of its bubbles)? We consider *dry* foams, *i.e.*, whose liquid content is less than  $\sim 1\%$  volume: these can be produced by allowing a freshly made foam to drain. They obey *Plateau’s laws* [6]:

1. Films meet at  $120^\circ$  angles at triple points.
2. The curvature  $\kappa$  of a film separating two bubbles balances the pressure difference between them (Laplace’s law). Hence each film is an arc of circle, and the sum of film curvatures (with an appropriate sign convention) at a triple point is zero.

Furthermore, we make the common assumption that the gas filling the bubbles is incompressible, and does not diffuse appreciably between bubbles: that is, we restrict ourselves to time scales intermediate between those of

<sup>a</sup> e-mail: paulo@ist.utl.pt

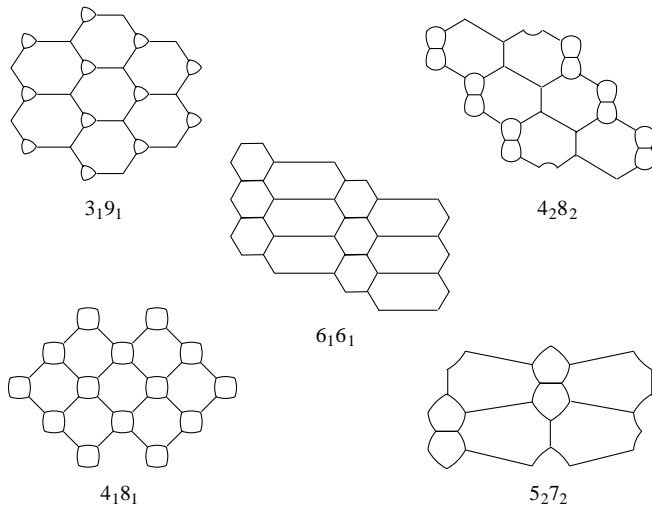


**Fig. 1.** The five mixed tilings that are minimal in some range of the bubble area ratio  $\lambda$ , from [7]. A simple notation is employed for these periodic structures, *e.g.*,  $4_1 8_1$  means “one four-sided bubble and one eight-sided bubble per unit cell”, etc.

drainage (seconds to minutes) and of coarsening and film breakage (minutes to hours or days). We do not offer any rigorous mathematical proofs of our statements: instead, we just write down what appear to us to be the most likely candidate structures and compare their energies. These include both “mixed” arrangements or “tilings” (where the two types of bubble form a periodic pattern) and “separated” or “sorted” arrangements (where there is segregation into regions containing only bubbles of one size, with a well-defined interface between them). Indeed, Plateau’s rules, although very general, do not give any clue about the global structure of a foam. To reformulate the problem in other words: given a foam cluster composed of equal (known) numbers of bubbles of two different areas, what is its lowest-energy configuration? In particular, do its bubbles prefer to mix or do they sort by size into two subclusters, and if the latter, what is the shape of these subclusters? We seek the answer to this question as a function of bubble number and area ratio.

This paper is organised as follows: in Section 2 we generalise an earlier study by two of the present authors on periodic (thus infinite) bidisperse tilings of the plane [7] by allowing for the possibility of “phase separation” into two “pure” (*i.e.*, monodisperse) infinite honeycombs. Then in Section 3 we address finite 2d foams: after identifying the likely geometries of the minimal mixed and sorted clusters (Sect. 3.1), we estimate their total energies (Sect. 3.2) and compare them (Sect. 3.3). Finally, in Section 4 we summarise our results and place them in the context of work on related systems.

## 2 Mixed and sorted infinite foams

The surface free energy of a 2d dry foam is  $E = P\gamma$ , where  $P$  is the total length of films and  $\gamma$  is the film tension. If, as we suppose,  $\gamma$  is constant, then energy minimisation is

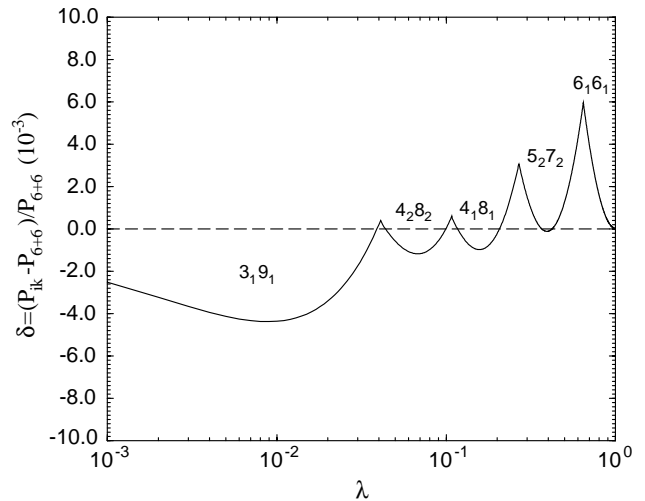


**Fig. 2.** Relative perimeter difference  $\delta$  between mixed and sorted bubble arrangements: the former are those of lowest energy in each range of  $\lambda$ , as labelled. The  $6 + 6$  sorted arrangement is favoured where  $\delta > 0$  whereas for  $\delta < 0$  the winner is one of the mixed arrangements.

**Table 1.** Minimal (*i.e.*, lowest-energy) arrangements *vs.*  $\lambda$  for infinitely large clusters. Tiling  $6_1 6_1$  never wins. Note the alternation between mixing and sorting.

Interval of $\lambda$	Minimal arrangements
0–0.039	$3_1 9_1$
0.039–0.044	$6 + 6$
0.044–0.099	$4_2 8_2$
0.099–0.117	$6 + 6$
0.117–0.206	$4_1 8_1$
0.206–0.367	$6 + 6$
0.367–0.421	$5_2 7_2$
0.421–1	$6 + 6$

equivalent to perimeter minimisation. In a recent paper, Fortes and Teixeira [7] identified the minimum-perimeter partitions of the plane for the special case where they are periodic and contain equal numbers of bubbles of areas 1 and  $\lambda$  ( $\lambda \leq 1$ , where  $\lambda$  is the area of the bubbles of smaller area —which turn out to have fewer sides), with  $1 + 1$  or  $2 + 2$  bubbles per unit cell, and such that all bubbles of the same size have the same topology. In order of increasing  $\lambda$ , they are (see Fig. 1):  $3_1 9_1$  (one 3-sided and one 9-sided bubble per period),  $4_2 8_2$ ,  $4_1 8_1$ ,  $5_2 7_2$  and  $6_1 6_1$  (notice that there is no  $5_1 7_1$  tiling); these results are exact. This set of tilings, satisfying Plateau’s laws [6], are likely to be the strongest candidates for perimeter minimisation. There are, of course, many more possibilities (*e.g.*, aperiodic tilings, or periodic with  $3 + 3$ ,  $4 + 4 \dots$  bubbles per unit cell), but for the sake of simplicity, and in order to concentrate on the physics of sorting, we restrict ourselves to the mixed tilings discussed in our earlier work [7].

We now enquire whether the mixed or sorted configuration has lower energy: how does the perimeter per pair of  $ik$  bubbles in a minimal mixed tiling,  $P_{ik}$ , compare with that of two separated honeycombs of bubble areas 1 and

$\lambda$ ,  $P_{6+6} = 2^{1/2}3^{1/4}(1 + \sqrt{\lambda})$ ? (Recall that the latter are the minimum-perimeter partitions of the plane in the case of monodisperse bubbles [3].) In Figure 2 we replot the results of Fortes and Teixeira for unbounded periodic tilings as  $\delta = (P_{ik} - P_{6+6})/P_{6+6}$  vs.  $\lambda$ .  $\delta$  is thus the relative perimeter difference between mixed and sorted configurations for a given  $\lambda$ , which is always less than 1%. It is striking that, as  $\lambda$  is increased, the absolute minimal configuration alternates (as shown by the changing sign of  $\delta$ ) between each of the above tilings (except  $6_16_1$ , which never wins), corresponding to  $\delta < 0$ , and the sorted arrangement,  $6 + 6$ , corresponding to  $\delta > 0$ . In particular,  $6 + 6$  wins for  $\lambda \lesssim 1$ , as predicted in [8]. Table 1 summarises which configuration has the lowest energy in each range of  $\lambda$ . These findings extend Morgan's [9] analysis of this minimisation problem: he did not consider tilings  $3_29_2$ ,  $4_28_2$  and  $6_16_1$ .

### 3 Mixed and sorted foam clusters

In finite clusters, boundary energies become important. These include the cluster's external boundary (*i.e.*, its outer surface in contact with the surrounding gas) and, in sorted clusters, also the interface between the two size-mismatched honeycombs. In the remainder of this paper we estimate the energy of the interface between such honeycombs and use it to determine the topology and geometry of the minimal configurations of finite 2d clusters composed of  $N$  bubbles of area 1 and  $N$  bubbles of area  $\lambda$ , as a function of  $N$  and  $\lambda$ . We then discuss the relation between the surface-energy-driven demixing and wetting behaviour of bubbles, as emerges from our work, and that of simple liquids: there turn out to be many points of contact, as well as some important differences.

#### 3.1 Candidate minimal clusters

The candidate minimal clusters that we consider are shown in Figure 3. They are of two main types: mixed (0) and sorted (I, II, III and IV).

Exact results for the bulk energy per pair of bubbles in the infinite mixed systems [7] have been reported above (see Fig. 2 and Tab. 1); we assume that it is the same for finite  $N$ , which is reasonable if  $N$  is large enough (say,  $N \gtrsim 10$ ). In the large- $N$  limit where the cluster can be treated as a continuous medium, it will minimise the energy of its outer boundary by being nearly circular (arrangement 0).

A sorted cluster consists of two monodisperse subclusters, each composed of hexagonal bubbles of areas 1 or  $\lambda$ : this minimises the total subcluster film perimeter for fixed bubble area in infinite clusters [3] and probably also for finite  $N$  [10]. In the large- $N$  limit, the energy per bubble is approximately the same as in a honeycomb, with a correction due to the boundaries. The optimal configuration minimises the total boundary energy: that of the interface between honeycombs plus that of all outer boundaries. Each such boundary is thus close to an arc of circle.

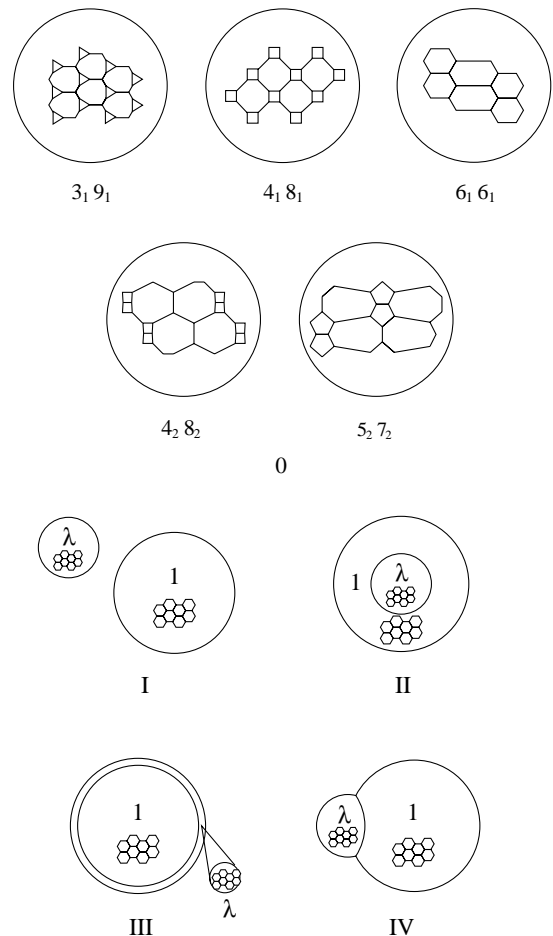


**Fig. 3.** The five mixed tilings (0) and the four sorted arrangements of honeycombs (I, II, III, IV) of bubble sizes 1 and  $\lambda$ . Note that in arrangements II and III the inner and outer clusters need not be concentric. In IV the honeycomb of bubble area  $\lambda$  “partially wets” that of bubble area 1: the resulting cluster satisfies “generalised Plateau laws” (*i.e.*, those that govern equilibrium of fluid films with different tensions). The mixed tilings are shown with straight sides for simplicity; see Figure 1 for a more accurate depiction.

In experiments, most clusters are seen to be fairly circular [11], and, if sorted, to consist of no more than two regions each made up of bubbles all of the same size [8]. Our candidates are therefore those that one might reasonably expect to be most often realised in practice: two separate circular clusters (arrangement I); circular clusters with either the cluster of smaller bubbles inside (arrangement II) or outside (arrangement III); and a cluster where one honeycomb “partially wets” the other, with circular outer boundaries and interface (arrangement IV). We do not hereby claim to have exhausted all possible cluster geometries: many more are conceivable, *e.g.*, clusters with “holes” (inner bubbles of pressure equal to that of the gas surrounding the cluster), non-circular clusters of special shapes, or clusters (*e.g.*, honeycombs) with defects (dislocations).

Clearly, III has higher energy than II, since the perimeter of their outer boundaries is the same, but that of the

internal interface is smaller in II. For that reason we do not consider III further: the serious candidates are thus 0, I, II and IV. Recall that their energies comprise bulk and boundary contributions, where the boundary energy is the sum of the outer boundary energy and the energy of the internal interface between clusters of bubbles of areas 1 and  $\lambda$ . To compute the energies of the various candidate arrangements we need to evaluate the contributions of the outer boundary of 0, I, II, and IV, and of the internal interface of II and IV. This is done in the next subsection.

### 3.2 Estimation of boundary energies

As mentioned above, we have calculated the total energy of each cluster as the sum of bulk and boundary energies. The bulk energy is  $N$  times the energy per bubble, already found exactly for the case of infinite clusters [7]. We now estimate the different boundary energies, or, equivalently, the energy per unit length:  $\gamma_S$  for the outer boundary, and  $\gamma_I$  for the interface between honeycombs. For dimensional reasons, both are proportional to the film tension  $\gamma$ , which fixes the energy scale of the problem.

For the energy of the outer boundary (per unit length of the boundary, and per unit length along the normal to the plane of the cluster),  $\gamma_S$ , we use the estimate of Fortes and Rosa [12]

$$\gamma_S \approx 0.576 \gamma, \quad (1)$$

for the orientation-averaged outer boundary energy of a finite honeycomb.  $\gamma_S$  in fact varies between  $0.522\gamma$  and  $0.604\gamma$ , depending on the orientation of the boundary, so  $0.576\gamma$  might seem an overestimation: a cluster should be able to lower its energy by adopting a special shape, *e.g.*, hexagonal, for which  $\gamma_S$  is smaller. Yet this is only possible for certain values of  $N$ , see, *e.g.*, [10]. Consequently, in the interests of generality we have opted for averaging  $\gamma_S$  over orientations, which gives us an upper bound on the outer boundary contribution to the cluster energy. Note also that  $\gamma_S$  is independent of the bubble size, and we neglect a possible dependence on topology [8]: all tilings, whether pure hexagonal or mixed, are assumed to have the same  $\gamma_S$ .

The interface between two honeycombs of bubble sizes 1 and  $\lambda \leq 1$  with parallel close-packed directions consists, for not too small  $\lambda$  (see below), of a wall of equispaced dislocations, which are pairs of adjacent bubbles with 5 sides (on the side of the honeycomb of bubble size  $\lambda$ ) and 7 sides (on the side of the honeycomb of bubble size 1). Figure 4 illustrates this with two real foam honeycombs for which there is no misorientation and  $\lambda \simeq 0.8$ ; note that the dislocations are unevenly spaced, implying that the interface is not at its energy minimum. In the appendix we obtain an average energy  $\gamma_I$  per unit length of the internal interface:

$$\frac{\gamma_I}{\gamma} = \frac{3}{\pi} \left( \frac{\sqrt{3}}{2} \right)^{1/2} \times \frac{1 - \sqrt{\lambda}}{\lambda} \left[ \frac{1 + \sqrt{\lambda}}{8\pi} \left( \frac{2}{\sqrt{3}} \right)^{1/2} \ln \left( \frac{\pi}{3} \frac{\sqrt{\lambda}}{1 - \lambda} \right) + \frac{E_c}{\gamma} \right]. \quad (2)$$

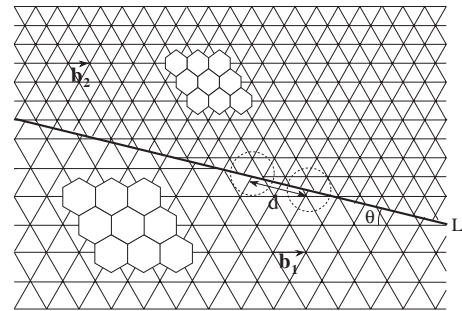
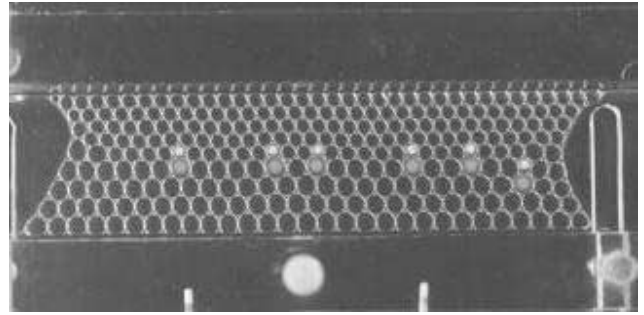


**Fig. 4.** Top: interface between two mismatched soap honeycombs, running approximately parallel to a close-packed direction; bubbles belonging to the 5–7 pairs are shown filled (courtesy of L. Afonso). Bottom: schematic representation of the wall of dislocations at the interface (thicker line) between honeycombs 1 and 2.  $b_i$  is the distance between the centres of adjacent hexagons in honeycomb  $i$ . The dashed circles are drawn around two adjacent dislocations, a distance  $d$  apart. Thinner lines denote the three close-packed directions in each honeycomb;  $\theta$  is the smallest angle between the interface and any of these directions.

The first term on the right-hand side of equation (2) is the elastic energy per unit length of the wall of dislocations, and per unit length perpendicular to the plane of the 2d cluster (in units of  $\gamma$ ). The second term is a core energy per dislocation, which we relate to the excess perimeter of a 5–7 pair of bubbles of areas  $\lambda$  and 1, respectively, relative to two hexagonal (*i.e.*, 6–6) bubbles of areas 1 and  $\lambda$ . To estimate  $E_c$  we use an equation derived by Graner *et al.* [8] relating the perimeter  $P_n$  and the area  $A_n$  of a single  $n$ -sided regular bubble with curved edges meeting at  $120^\circ$ :

$$P_n = c_n \sqrt{A_n}, \quad (3)$$

where  $c_n$  is a known numerical coefficient which is very weakly dependent on  $n$ . This yields

$$\frac{E_c}{\gamma} = \frac{1}{2} \left[ c_5 \sqrt{\lambda} + c_7 - (c_6 + c_6 \sqrt{\lambda}) \right]. \quad (4)$$

In Figure 6 below we plot  $\gamma_I/\gamma$  *vs.*  $\lambda$ . Its behaviour is similar to that of the energy of a low-angle grain boundary as a function of misorientation [13], with a maximum  $\gamma_I/\gamma \approx 0.0147$  at  $\lambda_{th} = 0.682$ . As in that case, the preceding analysis applies only when the dislocations are far enough apart to retain their individuality (*i.e.*, at large  $\lambda$ ).

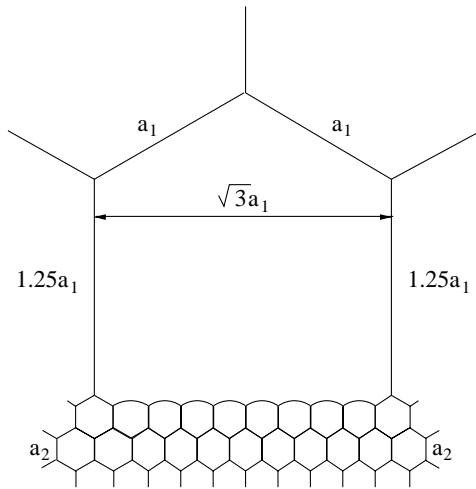


**Fig. 5.** Interface between two honeycombs of cell areas 1 and  $\lambda \ll 1$ . Cells of area 1 have a shorter perimeter at the interface than in the bulk—they are truncated. Cells of area  $\lambda$  located at the interface have approximately the same perimeter as they would at the outer boundary of a free cluster.

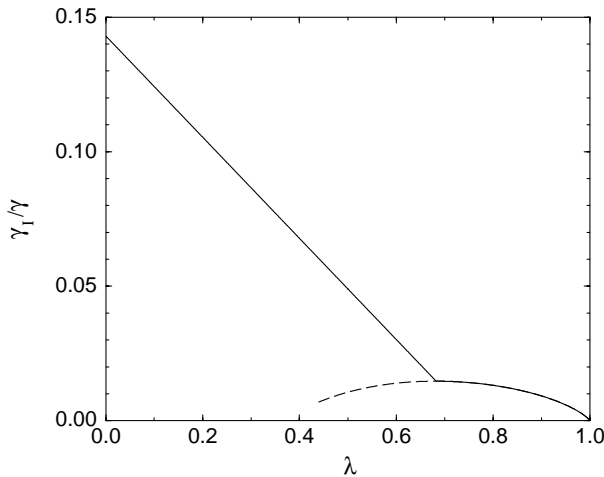


**Fig. 6.** Energy (in units of  $\gamma$ ) of the interface between two honeycombs,  $\gamma_I/\gamma$ , plotted as a function of area ratio  $\lambda$ . The dashed curve is the actual behaviour of equation (2) at small  $\lambda$ , where the approximations used to derive it break down; the straight portion of the solid curve is our linear interpolation between  $\lambda = 0$  and  $\lambda = \lambda_{th} = 0.694$ .

For larger misfits, *i.e.*,  $\lambda \leq \lambda_{th}$ , the interface will contain cells with numbers of sides other than 5, 6 or 7. We simplify the problem by estimating  $\gamma_I$  in the limit of very small  $\lambda$ , for which the interface will look as shown schematically in Figure 5 (see the appendix for details):

$$(\gamma_I)_{\lambda \rightarrow 0} = 0.143 \gamma. \quad (5)$$

Thus the interface energy increases from  $0.0147\gamma$  for  $\lambda = \lambda_{th} = 0.682$  to  $0.143\gamma$  for  $\lambda \simeq 0$ . For intermediate  $\lambda$  we interpolate linearly between these limits (see Fig. 6):

$$\frac{\gamma_I}{\gamma} = 0.143 - 0.188 \lambda \quad (\lambda < \lambda_{th}). \quad (6)$$

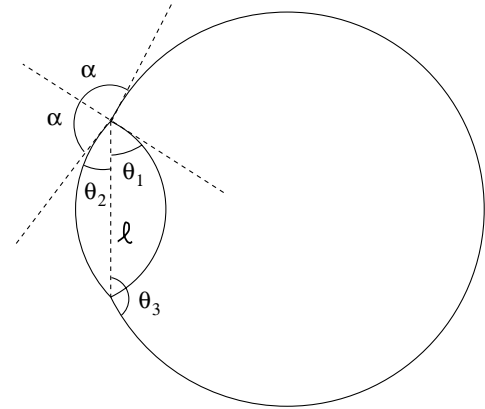


**Fig. 7.** Schematic representation of arrangement IV (the “partially wetting” honeycombs) in Figure 3, showing angles  $\theta_1$ ,  $\theta_2$ ,  $\theta_3$  between each of the films and the chord of length  $\ell$  at the triple points; and  $\alpha$ , such that  $2\alpha$  is the angle between films 2 and 3 at the triple points.

We can now compare the energies of sorted arrangements I, II and IV with that of a circular cluster (arrangement 0) inside which the  $2N$  bubbles are arranged in any of the minimal periodic tilings previously discussed.

### 3.3 Comparison of the energies of the different mixed and sorted arrangements

In what follows we use the estimates derived in the preceding section for the boundary energies  $\gamma_S/\gamma$  and  $\gamma_I/\gamma$ , and the exact results of [7].

For the mixed arrangements (0), we approximate the perimeter of a cluster of area  $N(1 + \lambda)$  by that of a circle of the same area,  $2\sqrt{\pi N}\sqrt{1 + \lambda}$ , and write

$$\frac{E_0}{\gamma} = NP_{ik} + 2\sqrt{\pi N}\sqrt{1 + \lambda} \frac{\gamma_S}{\gamma}, \quad (7)$$

where  $P_{ik}$  is, as before, the perimeter per pair of bubbles in the 1 : 1 (infinite) periodic tilings, which we take from [7].

The energies of each of the sorted configurations I, II and IV are obtained by adding together the internal energy ( $(2\sqrt{3})^{1/2} \sqrt{A} \gamma$  per bubble of area  $A$ ) and the boundary energies. We have

$$\frac{E_I}{\gamma} = (2\sqrt{3})^{1/2} N (1 + \sqrt{\lambda}) + 2\sqrt{\pi N} (1 + \sqrt{\lambda}) \frac{\gamma_S}{\gamma}, \quad (8)$$

$$\frac{E_{II}}{\gamma} = (2\sqrt{3})^{1/2} N (1 + \sqrt{\lambda}) + 2\sqrt{\pi N}\sqrt{1 + \lambda} \frac{\gamma_S}{\gamma} + 2\sqrt{\pi N}\sqrt{\lambda} \frac{\gamma_I}{\gamma}. \quad (9)$$

The minimum-energy configuration of type IV has circular boundaries meeting at two triple points at an angle  $2\alpha$  (see Fig. 7) given by

$$\cos \alpha = \frac{\gamma_I}{2\gamma_S}. \quad (10)$$

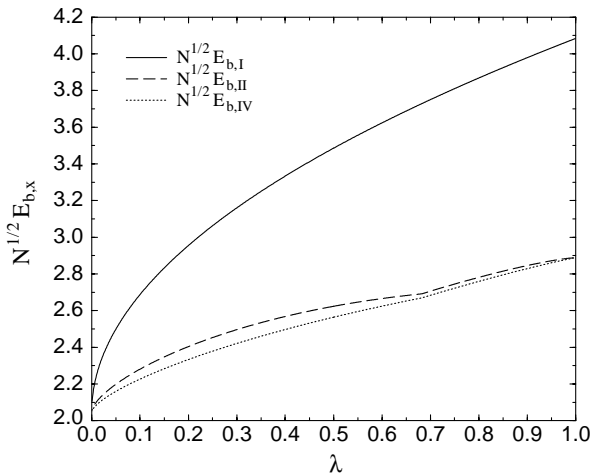


**Fig. 8.** Total boundary energy (outer boundary + internal interface) per pair of bubbles (of areas  $\lambda$  and 1) of sorted arrangement I (solid line), II (dashed line) and IV (dotted line). Arrangement IV has lower boundary (and also total) energy than the other two for all  $\lambda$ .

Now it follows from equations (1) and (6) that  $\gamma_I/\gamma_S \ll 1$ : the interface between honeycombs has a very low tension compared with that of the outer boundary, which implies  $\alpha \approx \pi/2$ . Then for  $\lambda$  not too small, the cluster will minimise its energy by having a nearly circular outer boundary. In addition, if  $\lambda \sim 1$  the interface between the two honeycombs will be a nearly straight line (a diameter in the limit  $\lambda \rightarrow 1$ ). The subtended angles  $2\theta_i$  of the three boundaries  $i$  ( $i = 1, 2, 3$ , see Fig. 7) are related to  $\alpha$  by

$$\theta_2 = \pi - \alpha - \theta_1, \quad (11)$$

$$\theta_3 = \pi - \alpha + \theta_1. \quad (12)$$

If  $\ell$  is the length of the common chord (shown as a dashed line in Fig. 7), the areas of the two regions each containing  $N$  bubbles of areas 1 and  $\lambda$  are

$$N\lambda = \ell^2 [G(\theta_2) + G(\theta_1)], \quad (13)$$

$$N = \ell^2 [G(\theta_3) - G(\theta_1)], \quad (14)$$

where

$$G(\theta) = \frac{\theta - \sin \theta \cos \theta}{4 \sin^2 \theta}. \quad (15)$$

For given  $N$  and  $\gamma_I/\gamma_S$  (or  $\alpha$  —or, ultimately,  $\lambda$ ), equations (11-15) determine  $\theta_i$  and  $\ell$ ; they were solved using MINPACK routine HYBRD [14]. The total energy of this configuration is then

$$\begin{aligned} \frac{E_{IV}}{\gamma} &= (2\sqrt{3})^{1/2} N (1 + \sqrt{\lambda}) \\ &+ \ell [F(\theta_2) + F(\theta_3)] \frac{\gamma_S}{\gamma} + \ell F(\theta_1) \frac{\gamma_I}{\gamma}, \end{aligned} \quad (16)$$

with

$$F(\theta) = \frac{\theta}{\sin \theta}. \quad (17)$$

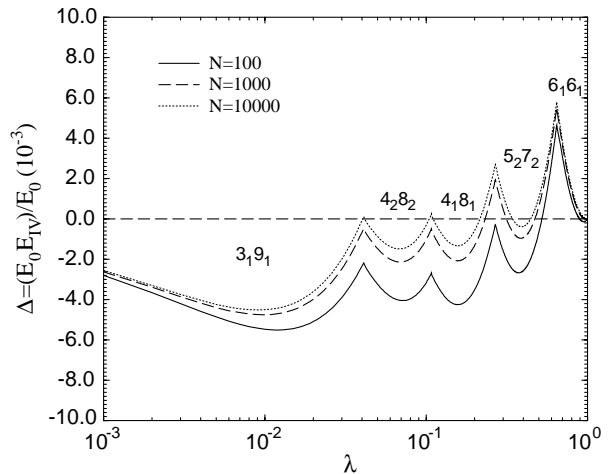


**Fig. 9.** Relative energy difference  $\Delta$  between mixed and sorted bubble arrangements, for clusters of different sizes. As  $N \rightarrow \infty$ , the results of Figure 2 for infinite systems are recovered.

Because all sorted arrangements have the same internal energy, we can subtract it out to define the *total boundary energy*  $E_{b,x}$  per pair of bubbles:

$$E_{b,x} = \frac{1}{N} \left[ E_x - (2\sqrt{3})^{1/2} N (1 + \sqrt{\lambda}) \right], \quad x = I, II, IV. \quad (18)$$

From equations (8-16) it is readily seen that  $E_{b,x}$  all scale with  $1/\sqrt{N}$ , so in Figure 8 we compare the *reduced* boundary energies  $\sqrt{N} E_{b,I}$ ,  $\sqrt{N} E_{b,II}$  and  $\sqrt{N} E_{b,IV}$ , which are independent of  $N$ . Arrangement IV —*i.e.*, the “partial wetting” geometry— always has the lowest energy, with that of arrangement II only very slightly higher. In fact, this could have been anticipated on the basis that IV is the only arrangement that satisfies “generalised Plateau laws” —the conditions for equilibrium of liquid films of unequal tensions: balance of pressures (implying circular boundaries) and balance of surface forces at triple junctions. Indeed, arrangement IV is the winner so long as it can exist, *i.e.*, up to  $\gamma_I/\gamma_S = 2$ , see equation (10). Otherwise the winner is II.

The above situation is in exact analogy with wetting at the interface between two immiscible liquids. A high surface tension  $\gamma_I$  leads to two separate droplets (complete dewetting, arrangement I). As  $\gamma_I$  decreases, the droplets are separated by an interface that is (in 3d) a spherical cap (partial wetting, arrangement IV), the angle of contact being determined by the balance of surface tensions (the “Neumann triangle”, corresponding to Young’s equation for the wetting of solids [15]). At even lower  $\gamma_I$  this equilibrium angle can no longer be defined, and one liquid (the one whose free surface —*i.e.*, that in contact with air— has lower tension) will wrap around the other, resulting in a spherical drop within another (complete wetting, arrangement II). If  $\gamma_I$  were negative, the two liquids would be miscible, and a single, large spherical droplet would be obtained (arrangement 0).

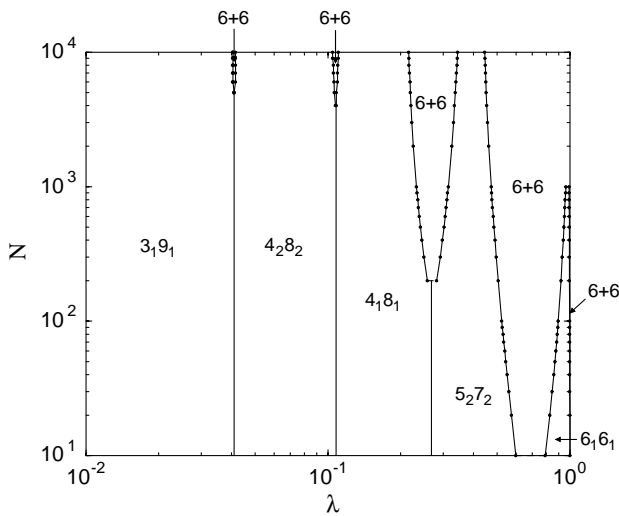


**Fig. 10.** “Phase diagram” of 1 : 1 bubble clusters in the  $(N, \lambda)$ -plane. The solid lines connecting data points are just to guide the eye; the short horizontal dashed lines show where the 6 + 6 regions approximately terminate, which has not been determined accurately. As  $N$  increases, the energy cost of forming an interface goes down and sorted (phase-separated) arrangements become favourable. In line with the approximations made, results are only meaningful for  $N \gtrsim 10$  (see the text for details). Note the very narrow 6 + 6 region for  $\lambda \lesssim 1$  (squashed against the right vertical axis).

In Figure 9 we track how the relative difference  $\Delta = (E_0 - E_{IV})/E_{IV}$  between the energy of the mixed arrangement, 0, and that of the lowest-energy sorted arrangement, IV, changes as a function of  $\lambda$  as  $N$  is increased. Smaller clusters want to be mixed on account of the high relative cost of forming interfaces; as  $N$  increases, “biphasic” regions appear. As expected [8], the  $6_1 6_1$  tiling is a stable structure of the smallest clusters to which our analysis applies, but loses out to the phase-separated honeycombs at large  $N$ . Convergence is however slow, and for  $N = 10^4$  we have not yet quite reached the  $N = \infty$  limit, *i.e.*, Figure 2 and Table 1. Figure 10 summarises these results as a “phase diagram” showing which is the most stable configuration (among those considered here) of foam clusters composed of  $N$  bubbles of area 1 and  $N$  bubbles of area  $\lambda$ .

## 4 Concluding remarks

We have addressed the mixing/sorting problem for foams composed of equal numbers  $N$  of bubbles of sizes 1 and  $\lambda$ , by estimating the energy cost of the interface between two honeycomb lattices. The minimum-energy configurations were found for any  $N$  large enough to justify employing the energy density of infinite periodic tilings of bubbles. Lowest-energy configurations of various topologies and geometries were identified as minimal for both finite and unbounded clusters. Such minimal configurations in general depend on  $\lambda$  as well as on  $N$ ; we have constructed the

**Table 2.** Likos and Henley’s winning phases *vs.*  $\lambda$  (from the second section of Tab. 2 in [16]). Where it exists, our notation for the same phase is given in brackets; they allowed for random tilings (RT), which we did not consider. Compare with Table 1.

Interval of $\lambda$	Minimal arrangements
0–0.024	$T_1^*$ ( $3_1 9_1$ )
0.024–0.089	$RT[(AB_2), (A)]$ (none)
0.089–0.154	$A + B(AB)$ (6 + 6)
0.154–0.171	$S_1(AB)$ ( $4_1 8_1$ )
0.171–0.192	$H_2(AB)$ ( $5_2 7_2$ )
0.192–0.393	$A + B(AB)$ (6 + 6)
0.393–0.417	$H_2(AB)$ ( $5_2 7_2$ )
0.417–1	$A + B(AB)$ (6 + 6)

corresponding phase diagram in the  $(N, \lambda)$ -plane (Fig. 10). We next summarise our conclusions.

1. The (least-energy) interface between two honeycomb lattices of different cell sizes has low energy compared with that of their outer boundary (at most,  $\gamma_I/\gamma_S \approx \frac{1}{4}$ ; recall that the outer boundaries of either honeycomb have the same energy per unit length). Consequently, the lowest-energy configuration of two sorted honeycombs is that where one “partially wets” the other (IV in Fig. 3).
2. On varying  $\lambda$  the minimal arrangement alternates between mixed (*i.e.*, single-phase) and sorted (*i.e.*, “phase-separated”). As predicted, mixing is favoured at small  $\lambda$  [7], while sorting wins for  $\lambda \simeq 1$  [8].
3. For  $N \gtrsim 1000$  the mixed  $6_1 6_1$  tiling ceases to be minimal for any  $\lambda$ .

How specific are these conclusions? Number 1 is a feature of size segregation: in species segregation, all boundary energies can be varied independently. Numbers 2 and 3 are intrinsic to the cellular nature of the foam and are not observed in the demixing of ordinary liquids. It is actually rather counterintuitive that a larger difference in bubble sizes should favour miscibility.

Here we considered just the special case of equal numbers of bubbles of each area, for which the stable “phases” are 6 + 6,  $3_1 9_1$ ,  $4_2 8_2$ ,  $4_1 8_1$  and  $5_2 7_2$ . The more general problem of finding the minimal configuration of clusters of bubbles of areas 1 and  $\lambda$  in any proportion would lead to the full phase diagram of “bubble alloys”. One such diagram has been reported by Likos and Henley [16] for a binary mixture of hard discs (in the  $N \rightarrow \infty$  limit): here too there is alternation between mixed and sorted arrangements, and even equilibria between mixed and pure phases [17]. Theirs, like ours, is a “zero-temperature” approach: both neglect the entropy. We collect their results for 1 : 1 clusters ( $p = 1/2$  in their notation) in Table 2; recall that in [16]  $r$  is the ratio of disc radii, hence  $\lambda = r^2$ . Although Likos and Henley included in their computations a larger number of candidate structures, the overall picture and cutoff values of  $\lambda$  are in rough agreement with ours; the main differences are: i) an interval where a “random tiling” wins; ii)  $5_2 7_2$  wins in *two* intervals; and iii) they did not consider  $4_2 8_2$ .

Another extension would be to address the same problem in 3d, which, as we saw, remains an open question even for monodisperse bubbles [18,19].

We do not, however, expect that a random collection of bidisperse bubbles will spontaneously relax towards its global energy minimum: as there is no thermal energy available (unlike in an atomic or molecular system), the cluster will most likely be trapped in a local minimum. Moreover, energy differences between minima are likely to be extremely small and hard to detect, requiring an extremely dry foam and very high-resolution image analysis. Direct experimental verification of the above predictions is thus probably not feasible, except perhaps by vibrating the foam as in the experiments of Fukushima and Ookawa [20,21].

Our patterns 0, I, II and III also occur in mixtures of biological cells, where they are likely to be a consequence of differences in intercellular energies [22]. The transitions between them have been simulated numerically [23], also in 3d [24], but are still not theoretically understood.

Finally, it is hoped that our work may be relevant to colloidal dispersions of particles interacting *via* soft repulsive potentials, which have recently been argued to obey a minimum-area principle [25]. Indeed, the configurations of model particle clusters is a topic of much current interest [26].

We thank L. Afonso for providing us with the photograph in Figure 4, C.N. Likos for correspondence, F. Morgan for a critical reading of the manuscript and many insightful remarks, M.E. Rosa for assistance with producing the line drawing in Figure 4, and M.F. Vaz for stimulating discussions. P.I.C. Teixeira acknowledges partial funding from the Fundação para a Ciência e Tecnologia (Portugal). F. Graner is grateful to Instituto Superior Técnico for its hospitality.

## Appendix A. Energy of the interface between two honeycombs of cell areas 1 and $\lambda$

We take two honeycombs, 1 and 2, of parallel close-packed rows of hexagonal cells of areas  $A_1 = 1$  and  $A_2 = \lambda \leq 1$ . Vector  $\mathbf{b}_i$ , connecting the centres of two adjacent hexagons of honeycomb  $i$ , has length  $b_i = \sqrt{3} a_i$ , where  $a_i$  is the cell side length.  $b_i$  is related to  $A_i$  by

$$A_i = \frac{\sqrt{3}}{2} b_i^2. \quad (\text{A.1})$$

The cases  $\lambda \simeq 1$  and  $\lambda \ll 1$  are treated separately below.

### Appendix A.1. Case $\lambda \simeq 1$

For  $\lambda \simeq 1$ , the misfit at the boundary is localised at equidistant, identical dislocations. These are 5–7 cell pairs, with the 5-sided cell in the smaller-cell honeycomb, 2. Each dislocation is associated with extra half-rows in honeycomb 2 (represented in the diagram of Fig. 4 by the lines that end at the interface). Consider a reference length

$L$  along the interface making an angle  $\theta$  with the close-packed rows ( $0 \leq \theta < \frac{\pi}{6}$  due to the sixfold symmetry): the numbers  $n_1$  and  $n_2$  of close-packed rows of a given family ending on either side of the interface are given by (see Fig. 4)

$$L \cos \theta = n_1 b_1 = n_2 b_2, \quad (\text{A.2})$$

whence

$$\frac{n_1}{n_2} = \frac{b_2}{b_1}. \quad (\text{A.3})$$

The number of dislocations (*i.e.*, extra half-rows of a given family) in  $L$  is  $n_2 - n_1$ . The repeat distance  $d$  between dislocations is then

$$d = \frac{L}{n_2 - n_1} = \frac{1}{\cos \theta} \frac{b_1 b_2}{b_1 - b_2}. \quad (\text{A.4})$$

Consider now a wall of dislocations with uniform spacing  $d$  and Burgers vector of length  $b$ , in an incompressible isotropic elastic medium of shear modulus  $\mu$ . The elastic field of the dislocation wall has range  $\sim d$ . The elastic energy per unit length along one dislocation is [13]

$$E_{\text{el}} = \frac{\mu b^2}{2\pi} \ln \frac{d}{r_c}, \quad (\text{A.5})$$

where  $r_c$  is the dislocation core radius. The total energy per unit area of the wall,  $\gamma_{\text{I}}$ , includes in addition the core energy per dislocation,  $E_c$ , and equals

$$\gamma_{\text{I}} = \frac{1}{d} \left[ \frac{\mu b^2}{2\pi} \ln \frac{d}{r_c} + E_c \right]. \quad (\text{A.6})$$

In the problem under discussion, we have a wall of dislocations at the interface between two media with different shear moduli  $\mu_i$ . For a honeycomb with inter-row spacing  $b_i$  we have [27]

$$\mu_i = \frac{\gamma}{2b_i}. \quad (\text{A.7})$$

We approximate the elastic energy of this non-uniform medium as the average of those of the two individual media 1 and 2, by replacing  $\mu b^2$  with  $(\mu_1 b_1^2 + \mu_2 b_2^2)/2$  in equation (A.6). We further take, for the core radius,

$$r_c = b_1 + b_2. \quad (\text{A.8})$$

Of course, in a cluster the interface can make any angle  $\theta$  with the close-packed rows. To take this into account, we calculate an average  $\gamma_{\text{I}}$  by first averaging  $1/d$  from equation (A.4) over  $\theta$  to obtain  $\langle 1/d \rangle$ , and then substituting  $\langle 1/d \rangle$  for  $1/d$  and  $\langle 1/d \rangle^{-1}$  for  $d$  in equation (A.6). This yields

$$\langle \cos \theta \rangle = \frac{6}{\pi} \int_0^{\frac{\pi}{6}} \cos \theta d\theta = \frac{3}{\pi}. \quad (\text{A.9})$$

Equation (2) then follows, which is valid for  $\lambda \simeq 1$ .

## Appendix A.2. Case $\lambda \ll 1$

For the interface shown in Figure 5,  $\gamma_I$  is the sum of two contributions. One is the excess energy of the smaller cells, which we approximate (per unit length) by  $\gamma_S$ , the average surface energy of a honeycomb, given by equation (1). The other is due to the reduction in perimeter of the larger cells at the interface: these are truncated hexagons of area 1, so their edges intersecting the interface have length  $1.25 a_1$  rather than  $a_1$ . The perimeter of one such cell is therefore  $4.5 a_1$  rather than  $6 a_1$ , hence each pair of larger cells contributes a negative perimeter of  $1.5 a_1$ , or  $0.75 a_1$  per cell. Since the interface length per larger cell is  $\sqrt{3} a_1$ , we obtain for  $\gamma_I$  in the limit  $\lambda \rightarrow 0$

$$(\gamma_I)_{\lambda \rightarrow 0} = \frac{0.576 \gamma \times \sqrt{3} a_1 - 0.75 a_1 \gamma}{\sqrt{3} a_1} = 0.143 \gamma. \quad (\text{A.10})$$

## References

1. D. Weaire, S. Hutzler, *Physics of Foams* (Oxford University Press, Oxford, 1999).
2. Marcus Terentius Varro, *On Agriculture* (Harvard University Press, Cambridge, MA, 1934).
3. T.C. Hales, *Discrete Comput. Geom.* **25**, 1 (2001).
4. W. Thomson (Lord Kelvin), *Philos. Mag.* **25**, 503 (1887).
5. D. Weaire, R. Phelan, *Philos. Mag. Lett.* **69**, 107 (1994).
6. J.A.F. Plateau, *Statique expérimentale et théorique des Liquides soumis aux seules Forces Moléculaires* (Gauthier Villars, Paris, 1873).
7. M.A. Fortes, P.I.C. Teixeira, *Eur. Phys. J. E* **6**, 133 (2001).
8. F. Graner, Y. Jiang, E. Janiaud, C. Flament, *Phys. Rev. E* **63**, 011402 (2001).
9. F. Morgan, *Trans. Am. Math. Soc.* **351**, 1753 (1999).
10. F. Graner, M.F. Vaz, S.J. Cox, C. Monnereau-Pittet, N. Pittet, unpublished.
11. M.E. Rosa, private communication.
12. M.A. Fortes, M.E. Rosa, *J. Colloid Interface Sci.* **241**, 205 (2001).
13. See, *e.g.*, W.T. Read, *Dislocations in Crystals* (McGraw-Hill, New York, London, 1953).
14. <http://www.netlib.org/minpack/hybrd.f>.
15. D.E. Sullivan, M.M. Telo da Gama, in *Fluid Interfacial Phenomena*, edited by C.A. Croxton (John Wiley, Chichester, 1986); F. Brochard-Wyart, in *La juste argile*, edited by M. Daoud, C. Williams (Les Editions de Physique, Les Ulis, 1995).
16. C.N. Likos, C.L. Henley, *Philos. Mag. B* **68**, 85 (1993).
17. Likos and Henley's discs do not fill space, but can be mapped onto a foam by means of a Voronoi construction on their centres. See Table 2 for the correspondence between their notation and ours.
18. D. Weaire (Editor), *The Kelvin Problem* (Taylor and Francis, London, 1997).
19. T. Aste, D. Weaire, *The Pursuit of Perfect Packing* (Institute of Physics Press, Bristol, 2000).
20. E. Fukushima, A. Ookawa, *J. Phys. Soc. Jpn.* **10**, 970 (1955).
21. E. Fukushima, A. Ookawa, *J. Phys. Soc. Jpn.* **12**, 139 (1957).
22. F. Graner, *J. Theor. Biol.* **164**, 455 (1993).
23. J.A. Glazier, F. Graner, *Phys. Rev. E* **47**, 2128 (1993).
24. J.A. Glazier, R.C. Raphaël, F. Graner, Y. Sawada, in *Interplay of Genetic and Physical Processes in the Development of Biological Form, Proceedings of Les Houches Conference 21-26 February 1994*, edited by D. Beysens, M.-A. Felix, G. Forgacs, F. Gail (World Scientific, Singapore, 1996).
25. P. Ziherl, R.D. Kamien, *J. Phys. Chem. B* **105**, 10147 (2001).
26. See, *e.g.*, J.P.K. Doye, arXiv:cond-mat/0007338 v2, and references therein.
27. M.E. Rosa, M. A. Fortes, *Philos. Mag. A* **77**, 1423 (1998).